IJIE

http://penerbit.uthm.edu.my/ojs/index.php/ijie
ISSN : 2229-838X e-ISSN : 2600-7916

The International Journal of Integrated Engineering

Numerical and Experimental Investigation of Aerodynamic Characteristics of Morphing Trailing Edge Wings in The Application of MAV

S Kishore Kumar[1*], Srinivas Pendyala[1]

[1]Department of Mechanical Engineering, Gitam School of Technology,
GITAM Deemed to Be University, Hyderabad, INDIA

*Corresponding Author

DOI: https://doi.org/10.30880/ijie.2023.15.05.009
Received 12 January 2023; Accepted 25 May 2023; Available online 19 October 2023

Abstract: In the past few years, FDM basedpolymer3D printing process has flourished mainly with ABS filaments as a thermoplastic source. Food packing, medical, marine and agriculture industries employdevices and other usable items made of polymers. Utilizing layered fabrication components in these areascompelthem to have self-cleansing, anti-freezing and corrosion resistant surfaces. It is generally complex and expensive to prepare hydrophobic coatings. The present work is related to the development of a surface coating on 3D printed ABS specimens with the mentioned properties. 3D printed specimens were fabricated using Flash Forge 3D printer without any modifications, and the hydrophobic coatings were achieved by dip coating process using Tricalcium phosphate-chitin solutions with a ratio of 70:30. Static contact angle measurement was employedin gaging wettability impact on dip coated 3D printed specimens. By using digital vernier calipers and profilometer (SJ410), dimensional accuracy and surface roughness were assessed pre and post-coating. According to ASTM D570-98, water absorption tests were conducted at different time intervals. Results of the experiment showed that the hydrophobic solutions had been successfully synthesized. The maximum contact angle was achieved for solution 1(4g of tricalcium phosphate solution with 0.3g chitin solution) i.e., 109.3°. Improvement in the textureof 3D printed ABS surfaceswasobserved after dip coating. Dip-coated 3D printed ABS specimens exhibited minimal absorption based on their weight gain per area.

Keywords: 3D printing, hydrophobic coating, surface roughness, dimensional accuracy, surface wettability

1. Introduction

Morphing wings have been discussed since the beginning of improved designs. Proposals and experiments originated primarily in the framework of improving aircraft products. Due to the general sophistication of existing flight and the constraints in terms of the energy consumed and therefore cost, morphing wings could primarily integrate better into modern aerospace applications properly. Going to lower-sized aircraft, where designs need to be more specified or described, makes morphing wing experiments far more possible. As a result, this article aims to explore specific morphing wing difficulties for micro aerial vehicle (MAV) two-dimensional wing models. A MAV is an air vehicle with a span of up to 60 cm and a weight of less than 200 g.

The ultimate focus is to adjust the wing's morphology dependent on flight situations to obtain the best potential shape by each flight condition. The morphed wing would be developed to enhance its aerodynamic characteristics by increasing the lift-drag ratio, which would be significant compared to enhancing lift and reducing drag. That information would minimize fuel usage and improve flight freedom. By modifying elements of the wing's characteristics, a morphed wing would permit the plane to fly at optimum lift-to-drag proportions for any situation experienced throughout flying. Aerodynamics and fluid control devices are examples of bioinspired engineering, which

*Corresponding author: ksandan@gitam.edu

applies ideas and concepts from nature to science and technology. According to numerous studies, an airplane wing's leading edge with a morphing design reduces smooth drag [1] [2].

Researchers identified various mechanical ways of achieving these required wings adaptabilities, and some ideas obtained important conceptual improved performance and over-estimate suggest. Nevertheless, the innovation was in its early development stages, and the innovation at the industry level still seems to need to be higher. However, only some concepts have progressed further to undertake wind tunnel tests, or even fewer have flown.Aircraft wing geometry modification through flight controls, requiring L.E. slats and T.E. flaps, has been commonly applied for lift and drag adjustment throughout the final approach. Because of hinge fairings and flap edge chambers, these mechanically operated elevated systems complicate the wing and are considered significant noisy generators. Morphing shapes that are lightweight and stay compliant with the wing were explored because they could enhance the performance of superior-lift systems. Its proposed morph techniques, like mechanical control units, adjust to variational flow situations by deformation rather than inflexible body movements, resulting in conforming structures and seamless structural surfaces [3].

The bird also flies its target at a speed between 5 and 10 m/s, equivalent to a flight Reynolds number between $3*10^3$ and $9*10^3$ based on an average chord length of 150 mm, The aerospace community is interested in enhancing micro air vehicles (MAVs) and extraterrestrial atmospheric flight vehicles (ETAFVs) whose cruise Reynolds number is in the range of 10^4.Plan-form modifications (swept tilt, span, and chord), out-of-airplane changes (twisting, dihedral, and span length bending), and airfoil alterations (camber and thickness) are the three basic types of wing morphing procedures. Morphing extensions were utilized to modify the wingspread and airfoil camber [4, 5], as well as the pitch and toe-nail angles of the winglets [6]and to restore conventional high-lift devices [7, 8].

Sanders et al. explored standard flap and adaptive changing following morphing trailing edges on the aerofoil. The conforming morph tail edge has been shown to have distinct aerodynamic advantages over the traditional physical flap. The difference in pressure over airfoil remained observed to rely on the structure of the distorted flight controls [9]. Daynes et al. (2012) observed a NACA 63-418 six-digit airfoil section with an asymmetric down-edge flap formation, including 20% of the chord length. They proved that the altering flaps produce the identical increase in lift force as a corresponding hinge flap with only around thirty percent of lower obtainable-of-level tips deviation [10]. Woods et al. (2014) performed wind tunnel investigations to examine the aerodynamics of the Fish Bone Active Curve morph shape and revealed that the maximum practicable lift-to-drag(L/D) ratio increases by 20 percent to 25 percent when compared to the original hinged trailing edge flaps [11]. In addition, Yokozeki et al. (2014) evaluated a morphed wing only using a seamlessly adjustable aileron utilizing a perforated construction in a wind tunnel and discovered that now the morphing wing has much less separation in flow and higher lift coefficient than a comparable conventional hinge wing [12].

Kamiya et al. performed various experimental and numerical investigations (Kamliya Jawahar et al., 2018) [13] employing a new T.E. (trailing edge) morphing idea established by Ai et al., 2016 and 2014 [15]. These analyses indicate that now the morphed-trailing-edge flap's curvature considerably changes the aerodynamic physical characteristics of an airfoil, resulting in significant improvements more than a conventional hinged-flap shape. Additionally, they observed that boosting the flapping deviation improves the effectiveness of a changing wing curvature. H. Kamliya et al. future an innovative metamorphosing tail operating efficiently utilizing a honeycomb core of axisymmetric varying rigidity and illustrated that trying to introduce variable resources into the varying bases might alteration of the controller source of an arrangement and enable customizing morphing characteristics, that either seriously influences the airflow and aeroacoustics efficiency of the airfoil sections [14, 15]. Kishore et al. discussed finalizing the morphing trailing edge airfoil section and its geometry two-dimensionally as on micro aerial vehicle conditions [16]. As the previous study indicates, many researchers have concentrated more on the structural characteristics of an evolving airfoil, with less consideration given to the aerodynamic and aeroacoustics performance. Previous studies, for example, show the actual aerodynamic appearance using the lift and drag ratio, with minimal reference to the aerodynamic performance. We provide the external Coefficient of pressure allocation and stream separation properties of the morphing airfoils inside this paper to realize better the streamlines properties in (MTE) morphed trailing edges methods. Additionally, the changes in airfoil are believed to decrease laminar turbulence. However, around is certainly not sufficient information behind this assertion.

This study details the results of a wind tunnel test campaign for an innovative morphing model established on a bio-mimic-inspired geometry and the capability to fly together with two-dimensional wing geometry differing in-flight situations. These tests examine the aerodynamic stream around the wing transforming or morphing. The Investigational Setup is represented using six-dimensional component balancing, and the flow field created by a morphing model was obtained experimentally. These tests were carried out using a low-speed wind tunnel at Aerodynamics Laboratory. A picture of the experimental setup is provided in Fig.1. The investigational arrangement is the morphing model, LSWT, a six-dimensional component forced to balance, and the aerodynamic performance of morphing two-dimensional wings. The results of a low-speed wind tunnel work for a new MAV's Micro air vehicle concept based on a bioinspired design and the ability to fly are presented in this study. The goal of this research is to investigate a bioinspired micro aerial vehicle with an adaptable wing test to confirm (morphing geometry) in three variable designs: morphing at deflections (without MTE deformation), morphing deflection angle 5^0 7^0 and 10^0 (MTE-semi-deformation) (maximum

deformation of the MTE). CATIA V5 tool was used to design the MTE-Morphing trailing edge wing, 3D printed with Polylactic Acid (PLA) material. Since the primary goal of this effort is to enhance the aerodynamic efficiency of Micro aerial vehicles, a proper investigation of experimental and numerical data for all angles of attack is required along with static morphed trailing edge profile models.

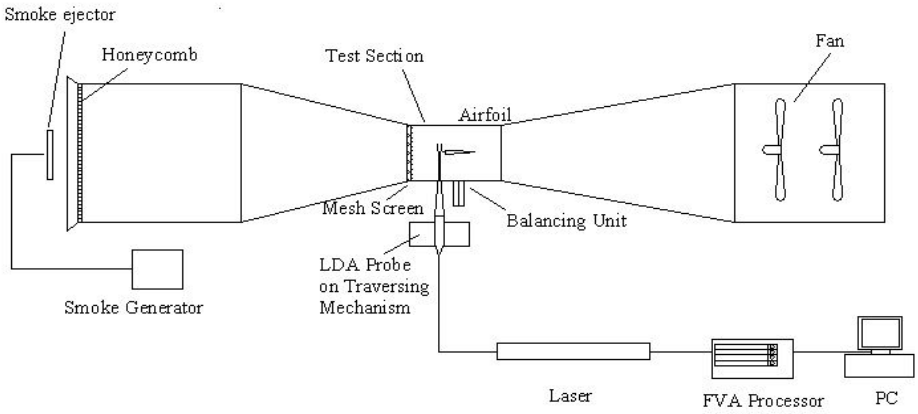

Fig. 1 - A schematic diagram of a Low-Speed Wind Tunnel (LSWT)

2. Methodology

2.1 Steady Geometry Parameterization

The twist in the best morphing airfoil discoveries is easily parametrized in a stable, static way. However, to run models through an active geometry twist approach, time must be introduced into the parametrization process to allow an unstable CFD analysis to yield results closer to real-world morphing. In this study, geometry will be parametrized using the Fish Bone Active Camber (FishBAC) idea (Woods et al., 2014b) [10], which will be adjusted for unstable morphing. The method's initial implementation used an essential way to represent a NACA 0018 wing enduring trailing edge deflections, commencing at 25 percent of chord trailing edge points and for varying maximum deflections. The standard airfoil was morphed by adjusting the slope configuration of the chord's chosen morphing area, then constructing a new airfoil shape using specific variable parameters. The morphing phase begins with a parameter specification, and the airfoil shape is created by aggregating the base NACA 0018 thicknesses dispersion and a parametrically determined camber line. Eq. 1 (Jacobs et al., 1933) defines the NACA 4-digit series thicknesses distribution.

2.2 Design and Model

A prototype developed and established on the NACA0018 and NACA23012 airfoil with a morphing T.E. were created to replicate the morphed wings analytically. Fig.2.2 (a) and (b) illustrate a morphed and traditional wing with a control surface flap. The morphing wing's morphing portion remains in the 25% minor chord of the aerofoil, while the static segment exists in the 15% major chord of the aerofoil. The position made by the chord length, as well as the line joining the deflecting axis to the T.E. (trailing edge), stands the morphed T.E. (trailing edge) by the deflected angle (δ), which varies between 0 to 10 degrees, with the downstream direction consistently favorable. V_1 is the freestream velocity, and alpha is the angle which is the chord length and direction of the velocity streamline of V_1.

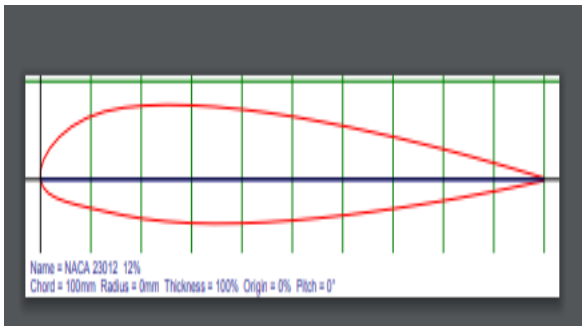

Fig. 2.1 - Selection of cad model of naca23012

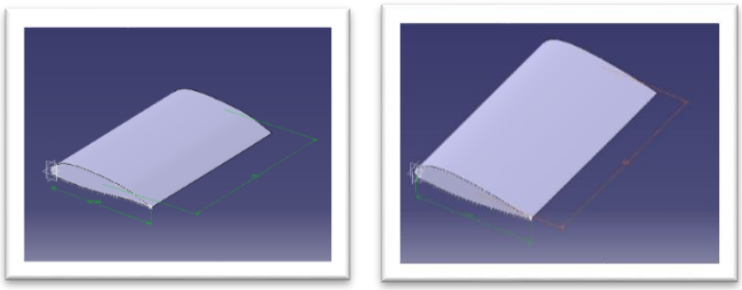

(a) (b)

Fig. 2.2 - CAD models (a) naca23012 and; (b) naca 0018 aerofoil

3. Aerodynamic Forces (L, D, and C_L/C_D)

3.1 Aerodynamic Characteristics

For a different range of flowing velocity as 5 m/s, 10m/s and 14.5 m/s as Reynolds number Re=34000, 68000 and 98600 respectively. The measurements of aerodynamic forceslift and dragfor a cambered airfoil with chord length (c)-100mm tailored with MTE-morphing trailing edges were agreed upon. The aerofoil was still examined for various angles of attack AoA from $0^0$to 16^0, along with identical MTE-morphed trailing edges and deflected angles of 5^0, 7^0, and 10^0. Instead of the three trailing edge camber forms of cases 1 through 4, the morphed trailing edge (MTE) with deflection angle (δ) = 5^0, 7^0, and 10^0 were explored.The experiments have remained performed employing a subsonic low-speed wind tunnel as shown in Fig.3(d) involving a convergency and differing outlet and a six-dimensional component balance set up as shown in Fig.3(b) to verify the accomplishment of changing two-dimensional wings. The description of the wind tunnel is represented in Table 1. Fig.3(c) shows the 6regulatesnent balance strain gauge: The balance force equipment, which is used to calculate the forces and moments from the balance setup, is required to mount all three aerodynamic forces and 3- moments like roll, yaw, and pitch that regulate a flight motion through the air. The prototype is fitted on a loop connected to the center. The left field position of the loop moves through with the back-end wall of the passageway and fastens to a weight gauge beyond the tunnel. The 6-d component balance is fixed inside the tabletop under the wind tunnel test section. Output from the 6-dimensional is maintained during a voltage along with strain gauges that converts the measurements interested in forces of data displayed on a desktop computer. Throughout the analysis, the angle of attack is w ide-ranging to provide a better implementation curve for the prototype. A few prototypes with quite a little type occurred examined in the low-speed wind tunnel. It is necessary to have the PLA (Polylactic Acid) prototypes for the shared airfoils, with chord and span lengths of 0.2 and 0.6 meters, respectively as shown in Fig.3(a). The prototypes were built with a smooth plane surface and coated finish to improve the accuracy of the results from aerodynamic effects. An airfoil is mounted on the test section, the current analysis assumes that the free stream velocity for comparable aerofoil is 10 ms^{-1}, The increasing air velocity, from 10 to 14.5 ms^1, was monitored.

Table 1 - Description of the Modest-Low speed wind tunnel

Specification	Value
Electric unit	III phase, 220 V AC 50 Hz/60 Hz (20 A)
Space requirement	2.5 m of free space around the inlet and 3 m at an outlet
Operating range in temperature	21 °C to 42 °C
Operational range relative humidity	60% at temperatures < 41°C decreasing linearly to 40% at 42°C.
Net sizes	3500 mm × 1000 mm × height 1600 mm
Dimensions of the current section (test section size)	0.6 m x 0.6 m x 2 m
Selection of airflow speed	0 to 50 m/s

3.2 Mounting the Morphed Trailing Edge (MTE) Airfoils Using 6D-Component Balance

The NACA 23012 aerofoil prototype (Fig. 2), which was produced using a 3D-controlled printing machine and had dimensions of a chord (c) = 0.1 m and span (s) = 0.6 m, was printed on a polylactic acid panel. The aerofoil was built with numerous compatible control surfaces for the trailing edge with the necessary slope shape and deflection angle (δ). The application of a new, aero acoustically and dynamically adaptable MTE surface. Four morphing trailing edges with camber profiles ranging from the simple flap to highly cambered conformal MTE were tested using a Java foil tool. These stayed in place for the ongoing, in-depth investigative research. According to Fig. 2, the morphing trailing edge deflection angle is the morphing deflection distance (b) ratio to the tip deflection (δ), with helpful bend angles in the pressure side direction. The airfoils MTE (morphed trailing edges) and variable camber forms intended for deflection angles of 5^0, 7^0, and 10^0, i.e., cases 1 through 4, were evaluated. The first case uses both tip angles and is analogous to a

traditional hinge surface movement. However, the following cases use conformal morphing trailing edge profiles that become increasingly cambered.

(a) (b) (c) (d)

Fig. 3 - Wind tunnel set-up (a) 3D-printed models; (b) strain guage balance platform; (c) 6-D component system; (d) LSWT

4. Computational Analysis

4.1 Geometry and Grid Generation

A variable trailing edge with the same structural element may achieve chord-wise and spanwise asymmetrical camber variation, resulting in a uniform shape with no excess gap. The NACA-23012 aerofoil through an adaptable trailed edge has been developed for numerical aerodynamic modeling in this experiment. The CFD method user-defined functions (UDFs) were used to investigate the aerodynamics of morphing two-dimensional wings, as grid domain shown in figure 4.1.

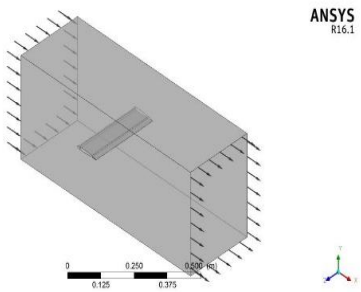

Fig. 4.1 Grid domain

4.2 CFD Plots at Various Velocities and Different Angles of Attack for Different Cases of MTE

4.2.1 Deflection Angle(δ)= 2^0, 5^0,7^0, and 10^0

From computational analysis, Fig.4.2 shows that the pressure is low at the leading-edge point at maximum pressure after morphing trailed edge deflections at 5 degrees. Moreover, Fig.4.3 shows the low-velocity profile after the morphing trailing edge at 5 degrees can predict that velocity should be shallow on the leading-edge aerofoil versus the trailing edge moving in under the morphing trailing edge surface. In case -3, the separation occurs on the pressure side. In contrast, in case-4, MTE edge airfoil at deflection at 7 degrees, the division is delayed by smooth profile due to MTE regaining energy to build the pressure at around 7 degrees, and the aerodynamic lift occurs maximum at the suction of trailing edge. As shown in Fig.4.4(a) and (b), the mesh at 14 degrees AoA converges. Improving the alpha (α) increases lift force and simultaneously rising drag along with the angle of attack-AoA due to the Morphing training edge. The Coefficient of drag decreases and improves the lift value. The Cl increases, causing an increment of lift-to-drag ratio, which reduces the flow of separation at MTE at 5 degrees and vortices trapped due to MTE-morphed trailing edge up to some deflections and delays the separation flow. In case -2, the MTE profile deflected at 7 degrees take place, and from Figure 4.5(a)since it can predict that the velocity increase from 5 $ms^{-1}$to 10 ms^{-1} compared towards MTE to the conventional airfoil. Figure 4.5 (b) illustrates the morphed trailing edge deflection at 5 degrees AoA at zero degrees for

a velocity of 10 m/s; the airfoil exhibits the high pressure created at the bottom of the surface because of the MTE at 5 degrees at AoA where the lift coefficient value increases along with the AoA- increases and stalls at 15 degrees but compare to MTE deflection of 5 degrees. Cl increases in value, and Cd rises as well, but as compared to the case, MTE deflection exhibits high cl and less drag. Overall lift-to-drag ratio performance and MTE airfoil for ten m/s velocities are improved. The value may rise or fall by raising the speed from 10 m/s to 14.5 m/s.

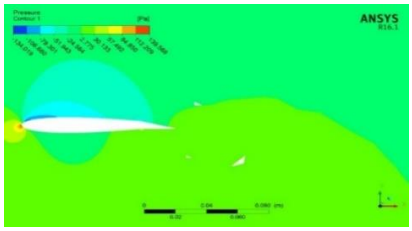

Fig. 4.2 - Pressure contour at deflection angle 50

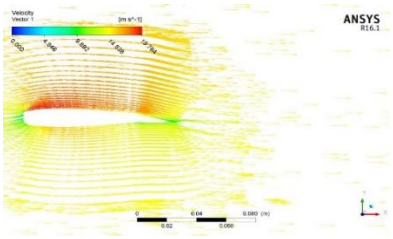

Fig. 4.3 - Velocity contour at deflection angle 50

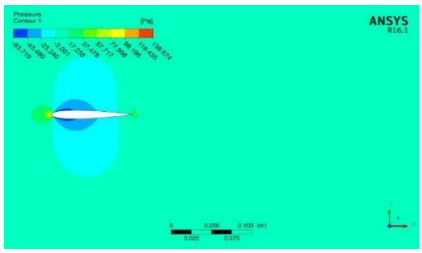

(a)

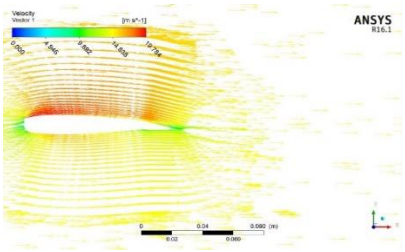

(b)

Fig. 4.4 - (a) And; (b) pressure contour and velocity contour at deflection at 7 degrees

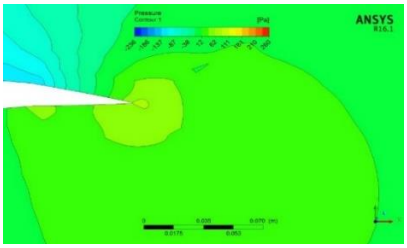

(a) Static pressure contour at MTE- (δ) = 5^0

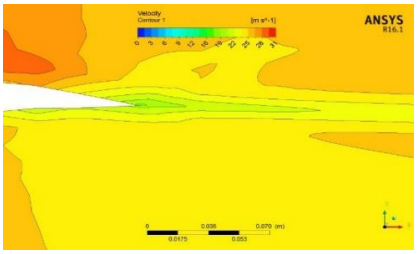

(b) Static velocity contour at MTE- (δ) = 5^0

Fig. 4.5 - (a) And; (b) NACA 23012 (MTE) morphing deflection angle of 5^0 for a flow velocity of 10 m/s

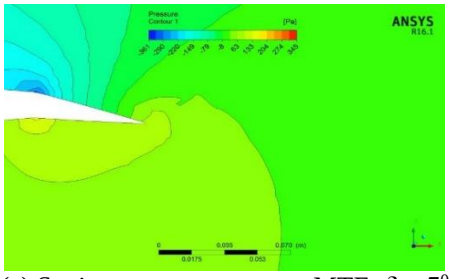

(a) Static pressure contour at MTE- δ = 7^0

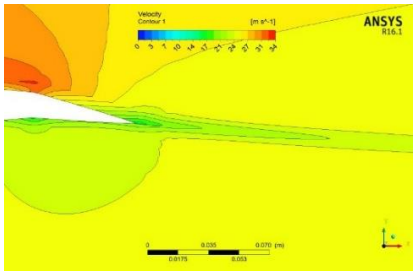

(b) Static velocity contour at MTE- δ = 7^0

Fig. 4.6 - (a) And; (b) static pressure and velocity contour over a (α) = 15^0 and MTE deflection angle of β = 7^0 for flow velocity of U = 10 m/s

The pressure suction is most significant at downward deflection compared to MTE- deflection at 5 degrees with the same Reynolds number, as shown in Fig. 4.6 (a) As shown in Fig.4.1.6(b), the pressure at morphing trailing edge deflection 7 degrees for velocity 10 m/s with Reynolds numbers is 68000. In terms of aerodynamic performance, as demonstrated in tables 3 and 4, the flow behavior alters to postpone the stall at higher deflection. It enhances the lift coefficient relative to MTE at 5 degrees. In a different scenario, figure 4.6 (b) depicts the velocity contours of the flow; it suggests that the velocity is lower at the lower surface than it is higher than at the upper surface due to a pressure difference at a specific point in the production of the lift value as shown in Fig. 4.7 for a given Reynolds number. It reenergized the flow to enhance the energy to produce more lift and lessen the drag force, creating the vortices at 7 degrees beneath the morphing trailing edge. According to the idea, morphing the trailing edge prevents or delays flow

separation and improves the lift-to-drag ratio (cl/cd). As shown in tables 3 and 4, increasing the angle of attack raises the lift value initially, but over time the lift stalls and increases the drag value. The Coefficient of lift and drag ratio is crucial for the micro aerial vehicle's aerodynamic performance.

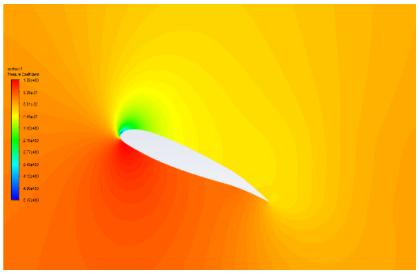

(a) Pressure contour at MTE δ=7 deg

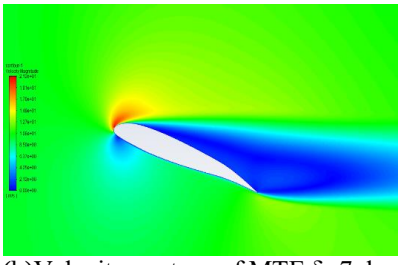

(b)Velocity contour of MTE δ=7 deg

Fig.4.7 - (a) And; (b) static pressure and velocity contour over a (α) = 160 and MTE deflection angle of β = 70 for flow velocity of U = 10 m/s

Table 4.1 - Without MTE deflection for a velocity=5 m/s

Airfoil	Velocity m/s	Angle of attack	Lift	Cl	Drag	Cd
NACA23012 ideal	2	0	2.64E-02	1.08E-02	1.59E-02	6.50E-03
		4	1.19E-01	4.87E-02	1.82E-02	7.42E-03
		8	2.00E-01	8.16E-02	2.46E-02	1.01E-02
		12	2.47E-01	1.10E-01	3.85E-02	1.57E-02
		14	2.56E-01	1.04E-01	4.88E-02	1.99E-02
		16	2.59E-01	1.06E-01	6.27E-02	2.56E-02

Table 4.2 - MTE deflection at 5 degrees for a velocity=10 m/s

Airfoil	Velocity m/s	Angle of attack	Lift	Cl	Drag	Cd
NACA23012 ideal	5	0	1.88E-01	1.23E-02	6.08E-02	3.97E-03
		4	8.28E-01	5.41E-02	7.10E-02	4.63E-03
		8	1.41E+00	9.20E-02	1.03E-01	6.74E-03
		12	1.78E+00	1.16E-01	1.80E-01	1.17E-02
		14	1.82E+00	1.19E-01	2.42E-01	1.58E-02
		16	1.76E+00	1.15E-01	3.34E-01	2.18E-02

Table 4.3 - MTE deflection at 7 degrees for a velocity=14.5 m/s

Airfoil	Velocity m/s	Angle of attack	Lift	Cl	Drag	Cd
NACA23012 ideal	10	0	8.00E-01	1.31E-02	1.61E-01	2.64E-03
		4	3.48E+00	5.68E-02	1.97E-01	3.22E-03
		8	5.97E+00	9.75E-02	3.17E-01	5.17E-03
		12	7.63E+00	1.25E-01	5.91E-01	9.67E-03
		14	7.78E+00	1.27E-01	8.25E-01	1.35E-02
		16	7.28E+00	1.19E-01	1.22E+00	1.98E-02

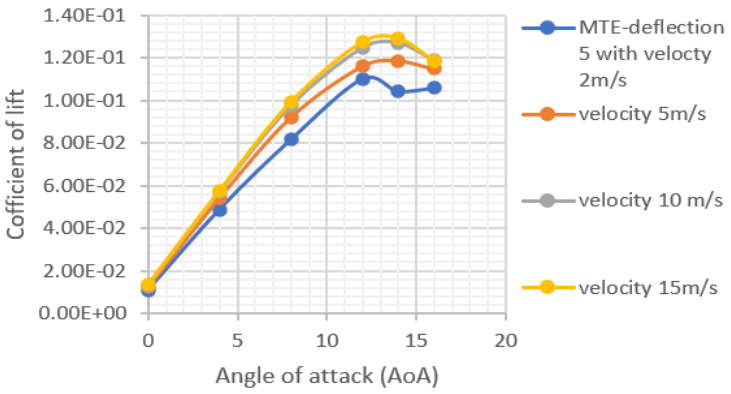

Fig.4.8 - Shows Coefficient of Lift (Cl) versus angle of attack (AoA) varying with different velocities

Table 4.4 - Shows the Coefficient of lift data for different MTE deflections δ=5, 7, and 10 degrees

NACA 2312 and Velocity-5 m/s				
Angle of attack	**Coefficient of Lift**			
Alpha	**without morphing**	**δ- 5 degrees**	**Del- 7 degrees**	**Del- 10 degrees**
0	1.227E-02	4.00E-02	5.77E-02	7.52E-02
4	5.408E-02	8.56E-02	9.77E-02	1.14E-01
8	9.202E-02	1.20E-01	1.30E-01	1.45E-01
12	1.161E-01	1.38E-01	1.48E-01	1.56E-01
14	1.186E-01	1.36E-01	1.43E-01	1.52E-01
16	1.148E-01	1.30E-01	1.42E-01	1.49E-01

Table 4.5 - Lift-to-Drag ratio efficiency of the morphing trailing edge for velocity=5 m/s

Angle of attack	**Coefficient of Lift -to Drag ratio**	
	conventional wing	**Morphing wing**
0	1.227E-02	4.00E-02
4	5.408E-02	8.56E-02
8	9.202E-02	1.20E-01
12	1.161E-01	1.38E-01
14	1.186E-01	1.46E-01
15	1.241E-01	1.49E-01
16	1.148E-01	1.20E-01

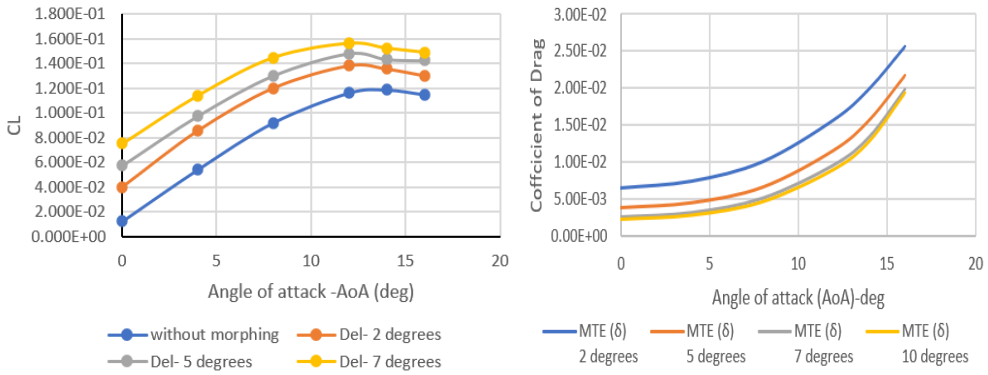

(a) (b)

Fig. 4.9 - (a) And; (b) shows Coefficient of Lift and drag versus angle of attack (α) varying with MTE (δ)=2, 5,7, and 10 degrees

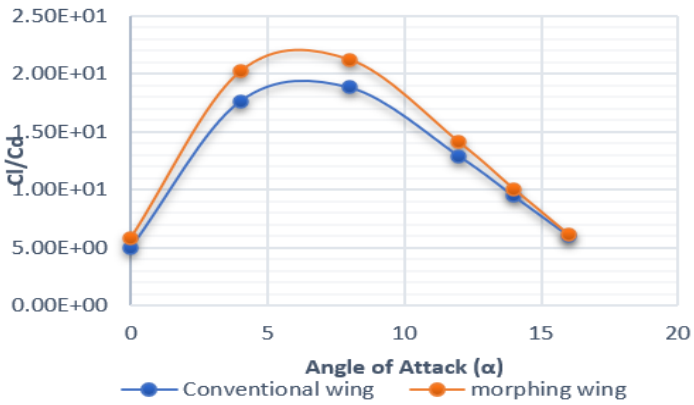

Fig. 4.10 - Lift-to-drag ratio for the conventional flap and morphed trailing edge airfoils with a deflection angle β=7 deg, at a freestream velocity of v=5 m/s

Results for the conventional and morphing airfoil's lift-to-drag coefficient ratios (Cl/Cd) are shown in Fig 4.10 and the results demonstrate a small, discernible change in Cl/ Cd between conventional and morphing airfoils. However,

when the angle of attack increases, the difference in Cl/Cd between the two scenarios gets smaller. For all the optimistic angles of attack, the Cl/Cd difference between the airfoils reduces to nominal values, as shown in Table 4.5. the data of cl, cd versus angle of attack for various profile tables4.3 and 4.4 displays the values of Cl and Cd. The performance of the conventional and morphing airfoils in terms of lift and drag is summarized in Fig.9(a) and (b), demonstrating that the conventional airfoils have higher Cl and Cd as the AoA-α increases, becoming uncomfortably near the stall point. Under the findings in the literature, investigations have also demonstrated that the deflection angle alters the stall angle compared to that conventional shape.

5. Experimental Analysis

A 3-D printer was used to develop and create the morphing two-dimensional wing model, which has dimensions of 0.6 m for the planform area span and 0.2 m for the chord. The prototypes must be built and covered with an aerodynamically smooth surface texture so that the results of the wind tunnel examination are more than precise. According to the research investigations, we have taken the span to be one and considered the chord length. An open subsonic wind tunnel test section of 0.6m*0.6m*0.2m is used for the aerodynamic experimental wind tunnel testing. Six-dimensional component balance, another piece of equipment that allows measuring aerodynamic forces in a wind tunnel, is used to obtain aerodynamic forces such as lift and drag moments and alter Reynolds numbers from and varying angle of attack from 0 degrees to 16 degrees. The aerodynamic forces and moments are implemented using the six-dimensional component balancing. The performance of CL with changing AoA is shown in Fig 5.4 coefficient of lift increases with the angle of attack. At maximum CL, stall occurs and beyond 12^0 AoA, the lift coefficient drops down. In contrast, the drag coefficient is inversely proportional to lift coefficient. Beyond stall angle, C_L increases and C_D decreases for an MTE deflection of 5^0. It is observed that the coefficient lift-to-drag ratio is maximum at 4^0 AoA and maintains a similar pattern for all the reynolds numbers. The maximum l/d ratio is observed for all the Reynolds numbers at an MTE of 7^0.

Fig. 5.1 - Low-speed wind tunnel

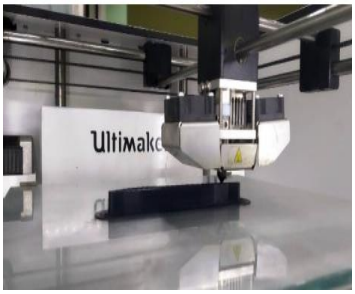

Fig. 5.2 - Three dimensional printing machine

(a)

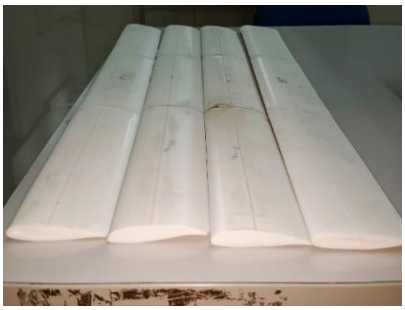

(b)

Fig. 5.3 - Two-Dimensional printed PLA Morphing trailing edges (MTE) models

According to the experimental investigation, we can see that for different MTE deflection angles of 5^0, 7^0, and 10^0, the coefficient of lift (Cl) increases as the AoA increases, as shown in Fig 5.4 Comparing the coefficient of lift data with other cases of MTE deflection at 5^0 and 10^0 and its maximum velocity at five m/s shows good agreement between the coefficient of lift data. In contrast, the lift coefficient dramatically increases upon the drag coefficient for various morphing trailing edges. Additionally, the drag coefficient rises along with cl and stalls at 14^0, as illustrated in Fig.5.5, following the drag sharply rising with the corresponding attack angle at its velocity of 5 m/s.

6. Assessment of the Computational and Experimental Analysis Results

To accurately comprehend the flow behavior across a morphing trailing edge with varied deflections at a given low Reynolds number or velocity at five m/s, as shown in Table 6.1, the following results for both computational and experimental study are provided. The computational result of the MTE at various deflection profiles is compared and validated with the experimental results. The values of the lift coefficient vary the angle of attack for different MTEs; after comparing the results, it is observed that the values of CL increase with MTE computationally and when compared to experimentally increasing deflection angles, the values show the same at the deviation of 1.5%. Observing the other MTE profile between computational and experimental, the results show similar deviations of 1.5 % as the deflection angles increase the aerodynamic efficiency changes, as shown in Fig.5.7. In terms of drag, when increases the deflection angle, it is observed that in the case of MTE 5^0, the drag curve shoots throughout stalling point.

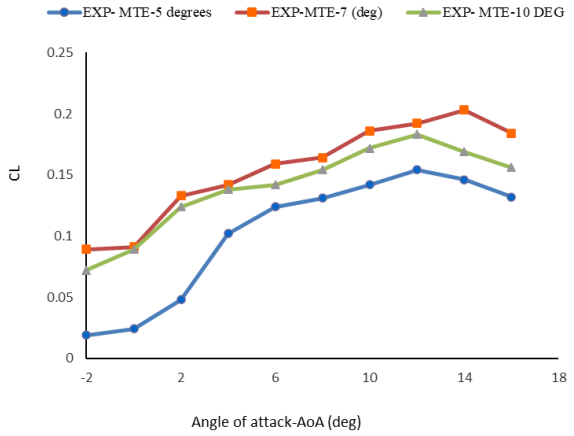

Fig 5.4 - Coefficient of Lift versus AoA (deg) varying MTE (δm) 5^0, 7^0 and 10^0 at Reynolds number 34000

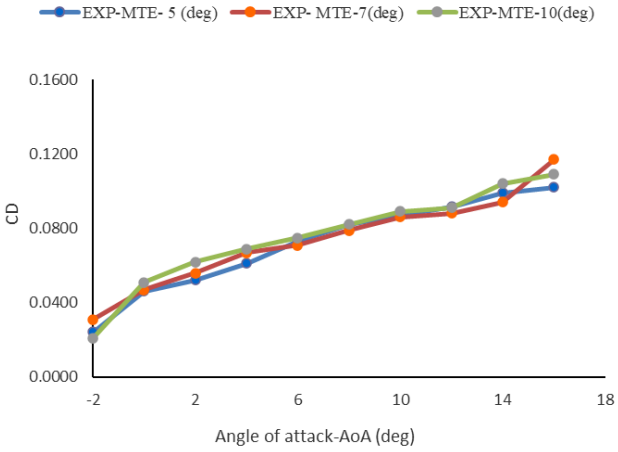

Fig 5.5 - Coefficient of Drag versus AoA (deg) varying MTE (δm) 5^0, 7^0 and 10^0 at Reynolds number 34000

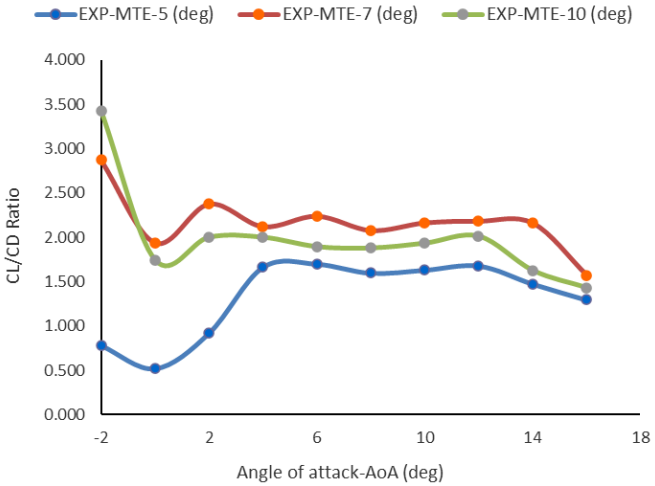

Fig 5.6 - Coefficient of Lift-to-Drag ratio versus AoA (deg) varying MTE (δm) 5^0, 7^0 and 10^0 at Reynolds number 34000

Table 6.1 - Experimental results - NACA 2312 airfoil with morphing trailing edge various deflections (MTE (δ)=5,7 and 10 degrees)

Angle of Attack	MTE-5^0		MTE-7^0		MTE-10^0	
α (deg)	Cl	Cd	Cl	Cd	Cl	Cd
-2	0.009	0.024	0.089	0.031	0.072	0.021
0	0.013	0.046	0.091	0.047	0.089	0.051
2	0.056	0.052	0.133	0.056	0.124	0.062
4	0.0974	0.061	0.142	0.067	0.138	0.069
6	0.124	0.073	0.159	0.071	0.142	0.075
8	0.131	0.082	0.164	0.079	0.154	0.082
10	0.142	0.087	0.186	0.086	0.172	0.089
12	0.154	0.092	0.192	0.088	0.183	0.091
14	0.169	0.099	0.203	0.094	0.169	0.104
16	0.152	0.102	0.184	0.117	0.156	0.109

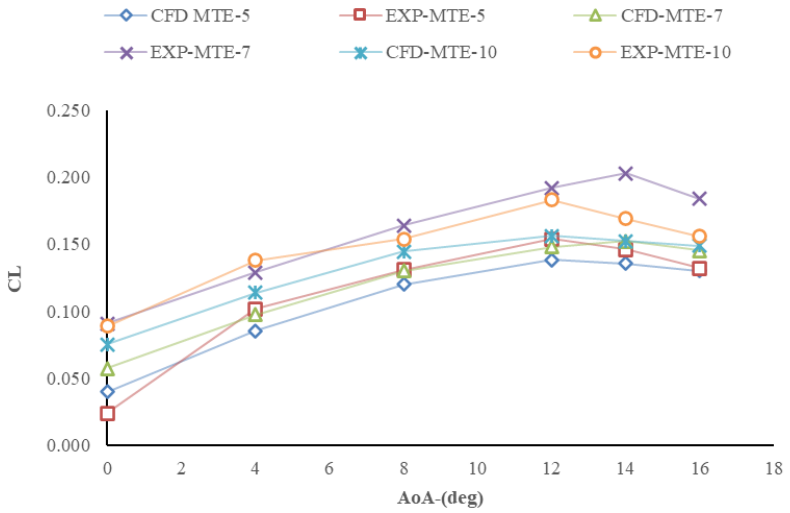

Fig. 5.7 - Comparison between computational and experimental data shows the lift coefficient versus AoA for various MTE (δm) 5^0, 7^0 and 10^0 at Reynolds number-34000

Fig.5.7 shows the coefficient of lift respective to the angle of attack on different morphed trailing edge profiles for different cases of deflection angles experimentally and computationally. The other side of Fig.5.8 shows the drag coefficient with the respective angle of attack(α) for various MTE-morphed trailing edge profiles for different cases of deflection angles. Compared with other MTE profiles, 7^0 gives good agreement in the result of Cl and less drag Cd, showing the same trend for results. Fig.5.9 shows the performance of aerodynamic efficiency lift to drag ration over an MTE on various deflection angles, the maximum lift-to-drag ratio values occurs AoA at 4 degrees give good agreement at MTE 7 degrees compare to other MTE deflection angles. For micro aerial vehicles maintains at AoA at 4 degrees and it good for gliding performance. The Cl and Cd with respective values of MTE for different profiles of deflection data are projected in tables 6.2 and 6.3 for experimental and computational. Fig. 5.9 compares aerodynamic efficiency between values of the coefficient of lift-to-drag ratio experimentally and computationally; here, the plot shows very clearly between the morphed trailing edge profile of all cases deflection at 5^0, 7^0, and 10^0. The cl/cd is quite an improvement in aerodynamic efficiency other than the MTE at 7^0 and 10^0compared with other deflections. Whereas the experimental results show the same trend and good aerodynamic efficiency compared with other deflections of MTE.

Table 6.2 - Comparison of Cd for experimental and computational results

	Experiment Results				Computational Results		
	MTE-5^0	MTE-7^0	MTE-10^0		MTE-5^0	MTE-7^0	MTE-10^0
AoA- (deg)	**Cd**	**Cd**	**Cd**	AoA(deg)	**Cd**	**Cd**	**Cd**
-2	0.024	0.031	0.021	-2	2.14E-03	1.52E-03	1.30E-03
0	0.046	0.047	0.051	0	3.97E-03	2.64E-03	2.30E-03
2	0.052	0.056	0.062	2	4.10E-03	2.91E-03	2.52E-03
4	0.061	0.067	0.069	4	4.63E-03	3.22E-03	3.25E-03
6	0.073	0.071	0.075	6	5.21E-03	4.21E-03	4.52E-03

8	0.082	0.079	0.082	8	6.74E-03	5.17E-03	4.94E-03
10	0.087	0.086	0.089	10	8.31E-03	8.12E-03	8.30E-03
12	0.092	0.088	0.091	12	1.17E-02	9.67E-03	9.02E-03
14	0.099	0.094	0.104	14	1.58E-02	1.35E-02	1.28E-02
16	0.102	0.117	0.109	16	2.18E-02	1.98E-02	1.93E-02

Table 6.3 - Comparison of Cl for experimental and computational results

Experiment Results				Computational Results			
	MTE-5^0	**MTE-7^0**	**MTE-10^0**		**MTE-5^0**	**MTE-7^0**	**MTE-10^0**
AoA-(deg)	**Cl**	**Cl**	**Cl**	**AoA-(deg)**	**Cl**	**Cl**	**Cl**
-2	0.009	0.089	0.072	-2	0..0021	0..0021	0..0035
0	0.013	0.091	0.089	0	0.04	0.0577	0.0752
2	0.056	0.133	0.124	2	0.06	0.0721	0.0931
4	0.0974	0.142	0.138	4	0.0856	0.0977	0.114
6	0.124	0.159	0.142	6	0.091	0.12	0.135
8	0.131	0.164	0.154	8	0.12	0.13	0.145
10	0.142	0.186	0.172	10	0.1298	0.137	0.1487
12	0.154	0.192	0.183	12	0.138	0.148	0.156
14	0.169	0.203	0.169	14	0.136	0.143	0.152
16	0.152	0.184	0.156	16	0.13	0.142	0.149

7. Conclusions

The aerodynamic performance of NACA 23012 airfoil with and without MTE of various profile shapes was investigated using experimental and theoretical techniques. The airfoil was tested at freestream velocities U=5 ms-1, 10 ms-1, and 14.5 ms-1, corresponding to the based Reynolds values. Aerodynamic force experiments have shown that the MTE (morphed trailing edge) with a highly cambered outline (Case-3 MTE-airfoil) produces higher lift than the simple other morphed trailing edge of cases-1, case-2, and case-4 for varying degrees of MTE profile with and without MTE. Despite the more significant coefficient of lift (cl) being recorded for the conclusion, the cl/cd data showed no discernible differences between the case-3 MTE airfoil and the without-MTE-case3 airfoil. The traditional airfoil suction peak is up to 30% lower than the MTE-case3 airfoil peak relative to low angles of attack, according to surface pressure measurements. The gap between the two narrows as the angle of attack rises. The angle of attack influenced the pressure distribution over MTE surfaces, which revealed significant differences between MTE airfoil instances. Flow measurement using a six-dimensional component balance is required to analyze the applications' stresses and moments of morphing trailing edges. Micro aerial vehicle conditions are used in tests to understand airfoils' aerodynamics and flow properties with conventional and morphing trailing edges. According to the results of the approach, a computational method was utilized to present the flow structures of the pressure and velocity contours for all MTE-morphing trailing edge circumstances with an angle of attack =0 to 16 degrees. These results led to the conclusion that the increased drag at low angles of attack may be related to the circulation and more excellent steady flow behavior displayed on the pressure side of the MTE case-3 airfoil, which is absent in conventional airfoils without MTE. These measurements show that minor modifications to the camber profile of MTE with deflections (δ) of 5 and 10 degrees can dramatically enhance the aerodynamic performance of airfoils.

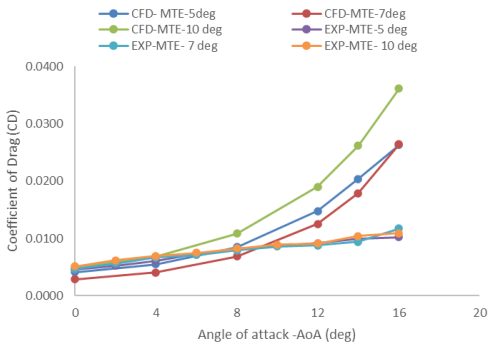

Fig. 5.8 - Shows experimental and computational results of coefficient of Drag versus AoA (deg) at Reynolds number=34000

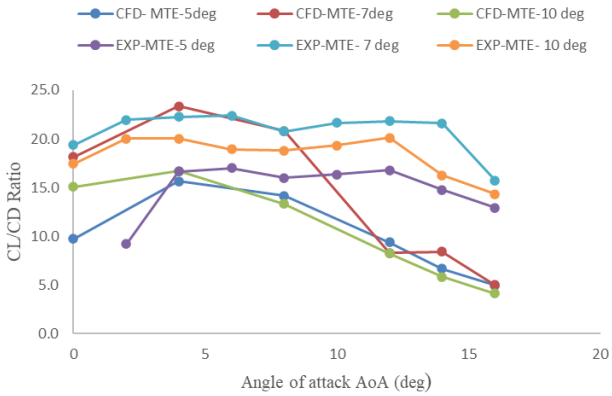

Fig. 5.9 - Shows experimental and computational results of CL/CD ratio versus AoA (deg) at Reynolds number=34000

Acknowledgement

The authors appreciate and recognize the support rendered by the staff of (LSWT) Aerodynamics wind tunnel laboratory, GITAM (Deemed to be University) Hyderabad to use of the facilities for study, data collection and analysis.

References

[1] S. Barbarino, O. Bilgen, R.M. Ajaj, M.I. Friswell, D.J. Inman: A review of morphing aircraft J. Intell. Mater. Syst. Struct., pp. 823-877, 22 (9) (2011).
[2] P. Gamboa, P. Alexio, J. Vale, F. Lau, A. Suleman, Design, and testing of a morphing wing for an experimental UAV, RTO-MP-AVT-146, Neuilly-sur-Seine, France, 2007.
[3] J. do Vale, A. Leite, F. Lau, A. Suleman Aero-structural optimization, and performance evaluation of a morphing wing with variable span and camber J. Intell. Mater. Syst. Struct., , pp. 1057-1073 , 22 (10) (2011).
[4] L. Falcao, A.A. Gomes, A. Suleman Aero-structural design optimization of a morphing wingtip J. Intell. Mater. Syst. Struct., pp. 1113-1124, 22 (10) (2011).
[5] G. Diodati, A. Concilio, S. Ricci, A. De Gaspari, C. Liauzun, J.L. Godard, estimated performance of an adaptive trailing-edge device aimed at reducing fuel consumption on a medium-size aircraft, in 8690-14, Smart Structures/NDE Conference, San Diego, CA, USA. 10–14 March 2013.
[6] R. Pecora, F. Amoroso, G. Amendola, A. Concilio Validation of a smart structural concept for wing-flap camber morphing Smart Struct. Syst. pp. 659-678, 14 (4) (2014).
[7] R. Pecora, F. Amoroso, L. Lecce Effectiveness of wing twist morphing in roll control J. Aircraft. pp. 1666-1674, 49 (6) (2012).
[8] Herr, M., and Dobrzynski, W., "Experimental Investigations in LowNoise Trailing-Edge Design," AIAA Journal, pp. 1167–1175. doi:10.2514/1.11101, Vol. 43, No. 6, 2005.
[9] Sanders B, Eastep FE, Forster E. Aerodynamic and aeroelastic characteristics of wings with conformal control surfaces for morphing aircraft. Journal of Aircraft;40(1):94–9, 2003.
[10] Daynes, S., Weaver, M.P., "A Morphing Trailing Edge Device for a Wind Turbine," Journal of Intelligent Material Systems and Structures, DOI: 10.1177/1045389X12438622, Vol. 23, No. 6, pp: 691-701, March 2012
[11] Woods et al., 2014 B.K. Woods, O. Bilgen, M.I. Friswell Wind tunnel testing of the fishbone active camber morphing concept J. Intell. Mater. Syst. Struct., pp. 772-785, 25 (7) (2014).
[12] Yokozeki et al., 2014 T. Yokozeki, A. Sugiura, Y. Hirano Development of variable camber morphing airfoil using corrugated Structure J. Aircraft, pp. 1023-1029, , 51 (3) (2014).
[13] Kamliya Jawahar et al., 2018 H. Kamliya Jawahar, M. Azarpeyvand, C. Silva Aerodynamic and Aeroacoustics Performance of Airfoils Fitted with Morphing Trailing-edges, 2018–2815, AIAA (2018).
[14] Ai et al., 2016 Q. Ai, H. Kamliya Jawahar, M. Azarpeyvand Experimental investigation of the aerodynamic performance of airfoils fitted with morphing trailing Edges, 2016–1563, AIAA (2016).
[15] Wolff, T., Ernst, B., Seume, J.R., "Aerodynamic Behaviour of an Airfoil with Morphing Trailing Edge for Wind Turbine Application," The Science of Making Torque from Wind 2014 (TORQUE 2014), DOI:10.1088/1742-6596/524/1/012018, June 2014.
[16] S. Kishore Kumar, Srinivas Pendyala, Numerical analysis of morphing wings for micro-aerial-vehicle application, Materials Today: Proceedings, Pages 2435-2439, https://doi.org/10.1016/j.matpr.2020.04.787, Volume 28, Part 4 May 2020.